ELSEVIER

Volume 181, Number 12, December 2008

JOURNAL OF SOLID STATE CHEMISTRY

www.elsevier.com/locate/jssc

CONTENTS

Abstracted/indexed in BioEngineering Abstracts, Chemical Abstracts, Coal Abstracts, Current Contents/Physics, Chemical, & Earth Sciences, Engineering Index, Research Alert, SCISEARCH, Science Abstracts, and Science Citation Index. Also covered in the abstract and citation database SCOPUS®. Full text available on ScienceDirect®.

Regular Articles

Syntheses, structures, and magnetic and optical properties of the compounds $[Hg_3Te_2][UCl_6]$ and $[Hg_4As_2][UCl_6]$
Daniel E. Bugaris and James A. Ibers
Page 3189

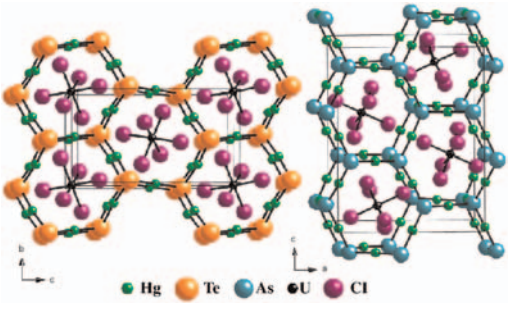

Views of the structures of $[Hg_3Te_2][UCl_6]$ and $[Hg_4As_2][UCl_6]$.

Phase separation, cation ordering and nano-structural complexities in $Nd_{2/3-x}Li_{3x}TiO_3$ with $x=0.14$
J.B. Lu, H.X. Yang, Z.A. Li, C. Ma, H.L. Shi, L.J. Zeng and J.Q. Li
Page 3194

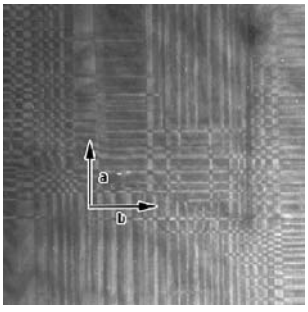

Transmission electron microscopy investigations on $Nd_{2/3-x}Li_{3x}TiO_3$ with $x=0.14$ reveal a rich variety of structural features in the samples prepared under different conditions, such as superstructures, anti-phase domains, one-dimensional lamella structure, nano-chessboard structures and circle-like pattern.

Regular Articles—Continued

Crystal and electronic structures, luminescence properties of Eu^{2+}-doped $Si_{6-z}Al_zO_zN_{8-z}$ and $M_ySi_{6-z}Al_{z-y}O_{z+y}N_{8-z-y}$ ($M=2Li$, Mg, Ca, Sr, Ba)
Y.Q. Li, N. Hirosaki, R.J. Xie, T. Takeda and M. Mitomo
Page 3200

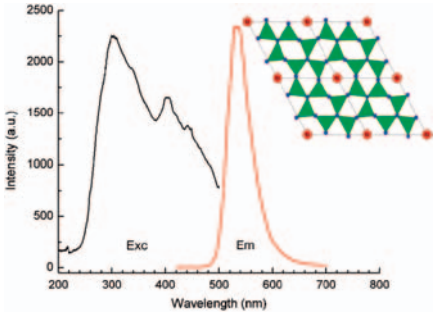

Excitation and emission spectra of $Eu_xSi_{6-z}Al_{z-x}O_{z+x}N_{8-z-x}$ with the project of a $2\times2\times2$ supercell crystal structure viewed along (001), in which red spheres are the Eu atoms.

Crystal structure and lattice dynamics of $Sr_3Y(BO_3)_3$
M. Mączka, A. Waśkowska, A. Majchrowski, J. Kisielewski, W. Szyrski and J. Hanuza
Page 3211

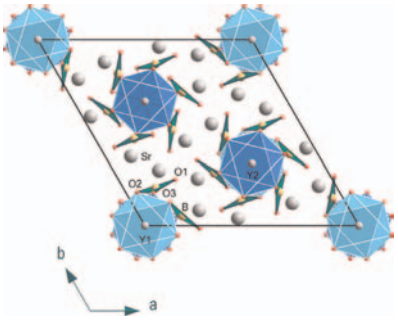

View of the crystal structure of BOYS along the *c*-axis.

Continued

Synthesis, physicochemical characterization and crystallographic twinning of Li_2ZnSnS_4
Jonathan W. Lekse, Beth M. Leverett, Charles H. Lake and Jennifer A. Aitken
Page 3217

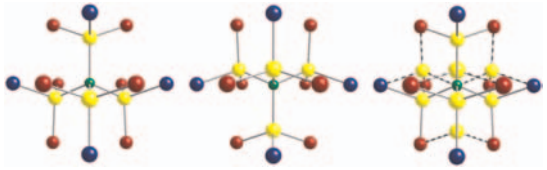

Li_2ZnSnS_4 is a new diamond-like semiconductor synthesized via high-temperature solid-state methods. Analysis of single-crystal X-ray diffraction data indicated that the structure was a pseudo-merohedral twin crystallizing in space group *Pn* and related to the wurtz-stannite structure. Additional characterization of the sample is reported.

Structure and magnetic properties of RE_2CuIn_3 (RE = Ce, Pr, Nd, Sm and Gd)
Yuriy B. Tyvanchuk, Andrzej Szytuła, Arkadiusz Zarzycki, Ute Ch. Rodewald, Yaroslav M. Kalychak and Rainer Pöttgen
Page 3223

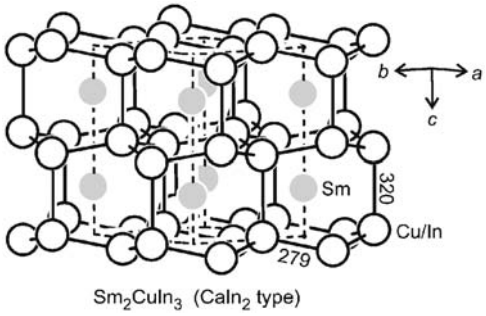

The $CaIn_2$-type structure of Sm_2CuIn_3.

***Ab-initio* crystal structure of hydroxy adipate of nickel and hydroxy subarate of nickel and cobalt from synchrotron powder diffraction and magnetic properties**
Adel Mesbah, Anne Carton, Lionel Aranda, Thomas Mazet, Florence Porcher and Michel François
Page 3229

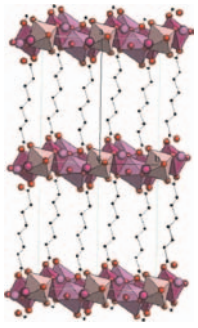

The hybrid metal-organic compounds $Ni(II)_5(OH)_6(C_6H_8O_4)_2$ **(1)**, $Ni(II)_5(OH)_6(C_8H_{12}O_4)_2$ **(2)** and $Co(II)_5(OH)_6(C_8H_{12}O_4)_2$ **(3)** have been synthesized by the hydrothermal route. The microporous metal hydroxide layers are bridged by dicarboxylates anions. **(1)** and **(2)** are antiferromagnetic with $T_N = 26.5$ and 19.3 K, respectively, while **(3)** is ferrimagnetic with $T_C = 16.2$ K.

X-ray and neutron powder diffraction studies of $Ba(Nd_xY_{2-x})CuO_5$
G. Liu, Q. Huang, J.A. Kaduk, Z. Yang, C. Lucas and W. Wong-Ng
Page 3236

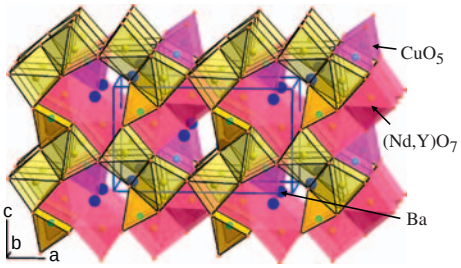

Perspective view of the "green phase" $Ba(Nd_xY_{2-x})CuO_5$ structure along the *b*-axis, showing the isolated square pyramids of $[CuO_5]$ and the trigonal prisms, RO_7, around the lanthanide sites.

Synthesis, crystal structure and NLO property of a nonmetal pentaborate $[C_6H_{13}N_2][B_5O_6(OH)_4]$
Huan-Xin Liu, Yun-Xiao Liang and Xiao Jiang
Page 3243

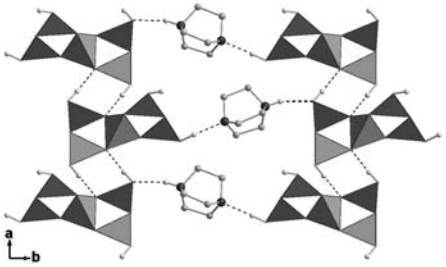

The protonated $[C_6H_{13}N_2]^+$ cations and the polyanions $[B_5O_6(OH)_4]^-$ form a 3D supramolecular network by extensive hydrogen bonds and electrostatic attraction. This compound shows NLO properties and the SHG efficiency is approximately 0.9 times that of KDP.

Controlled synthesis of nanocrystalline CeO_2 and $Ce_{1-x}M_xO_{2-\delta}$ (M = Zr, Y, Ti, Pr and Fe) solid solutions by the hydrothermal method: Structure and oxygen storage capacity
Preetam Singh and M.S. Hegde
Page 3248

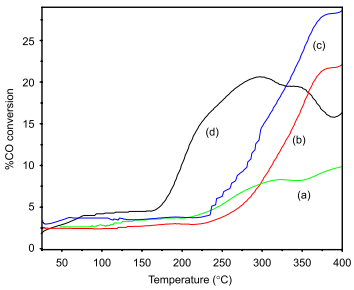

CeO_2 and $Ce_{1-x}M_xO_{2-\delta}$ (M = Zr, Ti, Pr, Y and Fe) nanocrystallites of 5–10 nm sizes have been synthesized by hydrothermal method using diethylenetriamine (DETA) and melamine as complexing agents. $Ce_{1-x}Fe_xO_{2-\delta}$ shows higher OSC and higher percentage of CO oxidation at lower temperature than $Ce_{1-x}Zr_xO_2$. CO conversion with lattice oxygen from (a) CeO_2 (5 nm), (b) $Ce_{0.75}Zr_{0.25}O_2$, (c) $Ce_{0.50}Zr_{0.50}O_2$ and (d) $Ce_{0.85}Fe_{0.15}O_{1.85}$.

Characterization of self-assembled films of NiGa layered double hydroxide nanosheets and their electrochemical properties

Ozge Altuntasoglu, Ugur Unal, Shintaro Ida, Motonobu Goto and Yasumichi Matsumoto

Page 3257

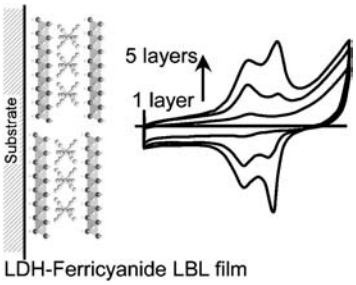

The thin film deposited from the nanosheets of ion-exchangeable NiGa LDH and ferricyanide molecule with LBL method gives the typical redox reaction of metal hexacyanoferrates in the interlayer. Current density depends on the number of layers.

Synthesis of nanocrystalline *RE*BO_3 (*RE* = Y, Nd, Sm, Eu, Gd, Ho) and YBO_3:Eu using a borohydride-based solution precursor route

Amanda E. Henkes and Raymond E. Schaak

Page 3264

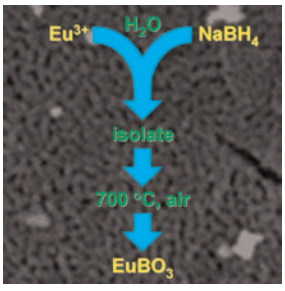

Amorphous nanoscopic precursor powders are formed through the aqueous reaction of RE^{3+} with $NaBH_4$. Once isolated, the powders can be annealed at 700 °C in air to form a series of nanocrystalline *RE*BO_3 orthoborates. Nanocrystalline YBO_3:Eu formed using this strategy shows red-orange emission properties when excited with UV light.

Synthesis, magnetism and electronic structure of $YbNi_{2-x}Fe_xAl_8$ ($x = 0.91$) isolated from Al flux

Xiuni Wu, Melanie Francisco, Zsolt Rak, T. Bakas, S.D. Mahanti and Mercouri G. Kanatzidis

Page 3269

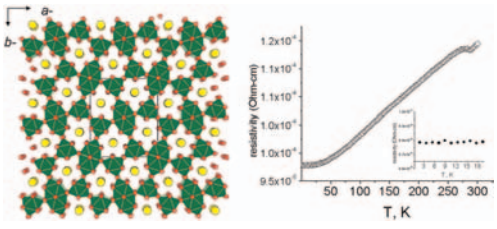

The reaction of ytterbium, nickel, iron in aluminum flux gives crystals of the intermetallic compound $YbNi_{2-x}Fe_xAl_8$ ($x = 0.96$) which adopts the $CaCo_2Al_8$ structure, *ab initio* electronic structure calculations within density functional theory using LDA + *U* approximation suggest an f^{13} configuration in the ground state.

Enhanced thermoelectric properties of bismuth sulfide polycrystals prepared by mechanical alloying and spark plasma sintering

Li-Dong Zhao, Bo-Ping Zhang, Wei-Shu Liu, Hai-Long Zhang and Jing-Feng Li

Page 3278

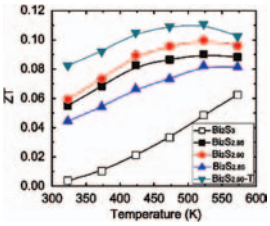

Electrical properties of bismuth sulfides were improved by optimizing carrier concentration through modifying compositions of sulfur and enhancing carrier mobility through SPSed hot-forging. The ZT value of 0.11 was obtained, which is the maximum reported so far.

Microscopic studies of a SnO_2/α-Fe_2O_3 architectural nanocomposite using Mössbauer spectroscopic and magnetic measurements

Naoaki Hayashi, Shigetoshi Muranaka, Shinpei Yamamoto, Mikio Takano, Dong-Feng Zhang, Ling-Dong Sun and Chun-Hua Yan

Page 3283

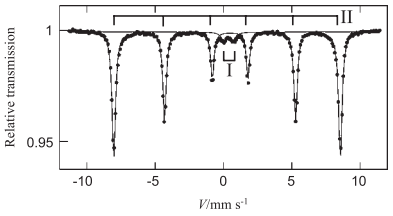

^{57}Fe Mössbauer spectrum of SnO_2/α-Fe_2O_3 architectural nanocomposite evidenced as SnO_2 nanorod arrays assembled on the surface of α-Fe_2O_3 nanotubes. (I: Fe-doped SnO_2 nanorods, II: α-Fe_2O_3 nanotubes) It was found for the SnO_2 nanorods that Fe^{3+} ions substituted slightly to $Sn_{0.998}Fe_{0.002}O_2$.

Predicted energies and structures associated with the mixed calcium strontium fluorapatites

Emily M. Michie, Robin W. Grimes, Shirley K. Fong and Brian L. Metcalfe

Page 3287

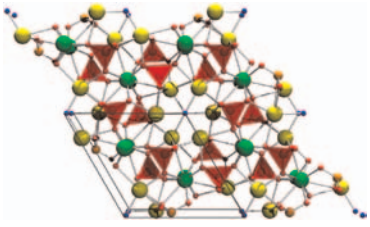

Quantum mechanical simulations rationalize the distribution of strontium and calcium over 6*h* and 4*f* cation sites in fluorapatite across the entire $Ca_xSr_{10-x}(PO_4)_6F_2$ solid solution. Lattice parameters and lattice volume are also analyzed as a function of Ca^{2+} and Sr^{2+} cation site distribution and concentration.

Continued

Substitution features in the isomorphous replacement series for metal-organic compounds $(Nb_xTa_{1-x})_4O_2(OMe)_{14}(ReO_4)_2$, $x = 0.7, 0.5, 0.3$—Single-source precursors of complex oxides with organized porosity
Olesya A. Nikonova, Vadim G. Kessler and Gulaim A. Seisenbaeva
Page 3294

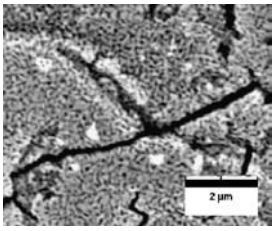

Thermal decomposition of $(Nb_{1-x}Ta_x)_4O_2(OMe)_{14}(ReO_4)_2$ ($x = 0.3$, 0.5, 0.7), single-source complex precursors, in air leads to the formation of crystalline solid solutions based on tantalum and niobium oxides, displaying semi-ordered pores with the size of 100–250 nm. In the dry nitrogen atmosphere, the decomposition leads to the formation of amorphous complex oxides containing rhenium, niobium and tantalum.

NMR evidence of LiF coating rather than fluorine substitution in $Li(Ni_{0.425}Mn_{0.425}Co_{0.15})O_2$
M. Ménétrier, J. Bains, L. Croguennec, A. Flambard, E. Bekaert, C. Jordy, Ph. Biensan and C. Delmas
Page 3303

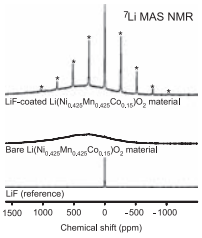

^{7}Li and ^{19}F MAS NMR show signals with isotropic positions characteristic of LiF, but with spinning sidebands envelopes characteristic of very strong dipolar interactions with the electron spins of the layered oxide, demonstrating that F is not a part of the material but is present as an LiF coating.

Solid chemistry of the Zn^{II}/1,2,4-triazolate/anion system: Separation of 2D isoreticular layers tuned by the terminal counteranions X ($X = Cl^-$, Br^-, I^-, SCN^-)
Sanping Chen, Shu Sun and Shengli Gao
Page 3308

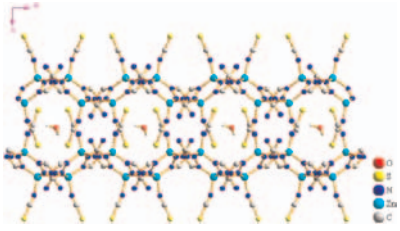

Based on employing the various terminal counteranions X ($X = Cl^-$, Br^-, I^-, SCN^-) the average interlayer separations of four 2D isoreticular layer compounds $[Zn(atrz)X]_\infty$ are gradually enlarged, which equal to 5.851, 6.153, 6.651 and 8.292 Å, respectively. As a result, guest H_2O molecules reside in the space between two adjacent layers of $[Zn_4(atrz)_4(SCN)_4 \tilde{n} H_2O]_\infty$.

Spin-glass-like behaviour in $IrSr_2RECu_2O_8$ (RE = Sm and Eu)
A.J. Dos santos-García, J. Van Duijn and M.Á. Alario-Franco
Page 3317

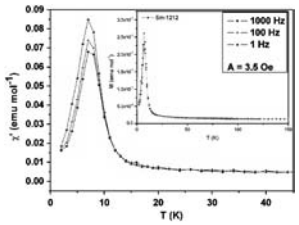

$IrSr_2RECu_2O_8$ with RE = Sm and Eu were prepared by high-pressure and high-temperature synthesis. Both samples adopt a M-1212-type perovskite structure and a microdomain texturing of the long c-axis is observed by TEM. A very interesting magnetic behaviour is observed in these materials. A "cluster by cluster freezing" model is proposed, instead of the classical individual spin freezing one to explain the spin-glass-like behaviour that seems to coexist with weak ferromagnetism in both compounds.

A two-fold interpenetrating 3D metal-organic framework material constructed from helical chains linked via 4,4′-H_2bpz fragments
Yi-Ming Xie, Zhen-Guo Zhao, Xiao-Yuan Wu, Qi-Sheng Zhang, Li-Juan Chen, Fei Wang, Shan-Ci Chen and Can-Zhong Lu
Page 3322

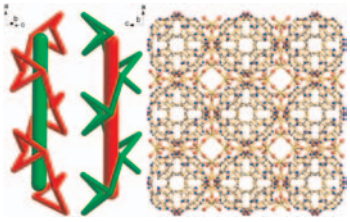

A 3-connected dia-f-type metal-organic framework compound $[Ag(4,4'\text{-bpz})_{3/2}H_2PO_4]$ shows unprecedented alternating left- and right-handed helices structure, featuring a non-uniform two-fold interpenetrated (4.14^2) net.

Influence of synthesis condition on product formation: hydrothermal auto-oxidated synthesis of five copper halides with ratio of Cu(I)/Cu(II) in 1:1, 2:1, 3:1, 4:1 and 1:0
Shuai Zhang, Yanning Cao, Hanhui Zhang, Xiaochuan Chai, Yiping Chen and Ruiqing Sun
Page 3327

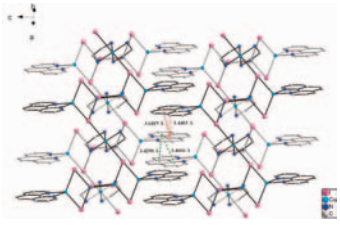

The influence of hydrothermal synthesis condition on the ratio of Cu(I)/Cu(II) of five copper iodides, with 1:0, 1:1, 3:1, 4:1, 2:1, respectively, is deduced and the rivalrousness of 1,10-phenanthroline, ethylenediamine and 1, 3-propanediamine is discussed as well. The fluorescent study shows **1** exhibits intense orange-red luminescence with long lifetime ($\tau = 1.25$ μs) at 293 K and more intense emission and longer lifetime($\tau = 6.95$ μs) at 77 K.

Synthesis, crystal structure, and property of one- and two-dimensional complexes based on paradodecatungstate-B cluster

Bao Li, Lihua Bi, Wen Li and Lixin Wu

Page 3337

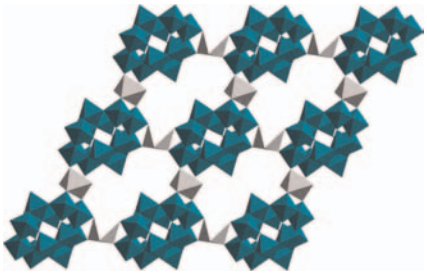

Three transition metals supporting complexes based on paradodecatungstate-B anions were obtained in aqueous solution. The single-crystal structure analysis reveals that two of them are one-dimensional while the other one is a two-dimensional complex.

Synthesis, phase transition and photoluminescence studies on Eu^{3+}-substituted double perovskites—A novel orange-red phosphor for solid-state lighting

V. Sivakumar and U.V. Varadaraju

Page 3344

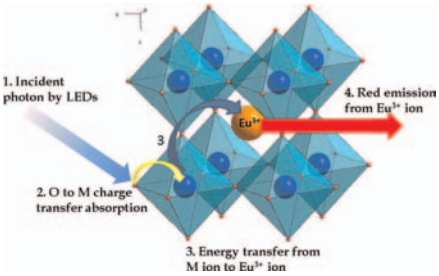

A series of orange-red-emitting A_2CaWO_6 (A = Sr, Ba) and $Sr_{1.9-x}Ba_xEu_{0.05}Li_{0.05}MoO_6$ (x = 0–1.9) phosphor with double perovskite structure have been synthesized by solid-state reaction. All the compositions show broad charge transfer band and orange-red [magnetic dipole (MD) and electric dipole (ED)] emission. The red emission of $Sr_{1.5}Eu_{0.05}Li_{0.05}Ba_{0.4}CaWO_6$ is found to be ~4.5 times higher than that of commercial red phosphor (Nichia) under 465 nm excitation and hence this phosphor could be a potential candidate for white LED based on blue/NUV GaN LED.

Synthesis, Raman and Rietveld analysis of thorium diphosphate

Nicolas Clavier, Gilles Wallez, Nicolas Dacheux, Damien Bregiroux, Michel Quarton and Patricia Beaunier

Page 3352

The cubic structure of ThP_2O_7, built of ThO_6 octahedra and P_2O_7 ditetrahedra.

Formation of titanium phosphate composites during phosphoric acid decomposition of natural sphene

Marina V. Maslova, Daniela Rusanova, Valeri Naydenov, Oleg N. Antzutkin and Lidia G. Gerasimova

Page 3357

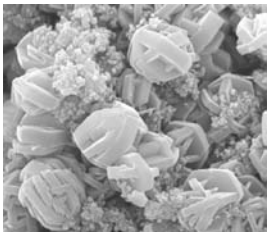

A new synthesis scheme for preparation of composite titanium phosphate (TiP) ion-exchangers upon one-stage decomposition process of natural sphene with phosphoric acid is presented. Syntheses of α-TiP–silica composites proceed via formation of meta-stable titanium phosphate phases. The concentration of H_3PO_4 determines the porosity of final products and their sorption affinities.

Synthesis, crystal structure and magnetic properties of a new pillared perovskite $La_5Mo_{2.75}V_{1.25}O_{16}$

Farshid Ramezanipour, Shahab Derakhshan, John E. Greedan and Lachlan M.D. Cranswick

Page 3366

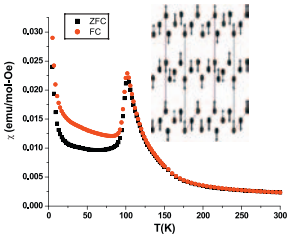

Long-range magnetic order below 100 K in the pillared perovskite $La_5Mo_{2.75}V_{1.25}O_{16}$. The magnetic structure is shown in the inset.

Rapid Communication

Adsorption of arsenic(III) into modified lamellar Na-magadiite in aqueous medium—Thermodynamic of adsorption process

Denis Lima Guerra, Alane Azevedo Pinto, Claudio Airoldi and Rúbia Ribeiro Viana

Page 3374

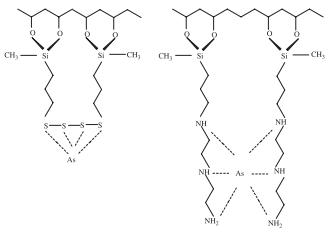

The results suggest that the adsorption capacities increased with an increase of reactive basic centers in the pendant organic chains of the intercalated agent.

Continued

Author inquiries

Submissions

For detailed instructions on the preparation of electronic artwork, consult the journal home page at http://authors.elsevier.com.

Other inquiries

Visit the journal home page (http://authors.elsevier.com) for the facility to track accepted articles and set up e-mail alerts to inform you of when an article's status has changed. The journal home page also provides detailed artwork guidelines, copyright information, frequently asked questions and more.

Contact details for questions arising after acceptance of an article, especially those relating to proofs, are provided after registration of an article for publication.

Language Polishing

Authors who require information about language editing and copyediting services pre- and post-submission should visit http://www.elsevier.com/wps/find/authorshome.authors/languagepolishing or contact authorsupport@elsevier.com for more information. Please note Elsevier neither endorses nor takes responsibility for any products, goods, or services offered by outside vendors through our services or in any advertising. For more information please refer to our Terms & Conditions at http://www.elsevier.com/wps/find/termsconditions.cws_home/termsconditions.

For a full and complete Guide for Authors, please refer to *J. Solid State Chem.,* Vol. 180, Issue 1, pp. *bmi–bmv*. The instructions can also be found at http://www.elsevier.com/wps/find/journaldescription.cws_home/622898/authorinstructions.

Journal of Solid State Chemistry has no page charges.